Original Article

Asian Pacific Journal of Tropical Biomedicine

apjtb.org

doi: 10.4103/apjtb.apjtb_451_25

Gracilaria chorda-derived compounds improve lipid metabolism and insulin sensitivity in 3T3-L1 adipocytes and high-fat diet-induced obese zebrafish larvae

Laxmi Sen Thakuri[1,2], DucDat Le[3], Hyun Jung Kim[4], Jung Jin Kim[1], Jong Bae Seo[1,5], Jong Cheol Park[6,7], Mina Lee[3]✉, Dong Young Rhyu[1,5]✉

[1]*School of Food and Pharmaceutical Engineering, Mokpo National University, Jeonnam 58554, Republic of Korea*

[2]*Bio-medicine Advanced Formulation Research Center, RLRC, Mokpo National University, Jeonnam 58554, Republic of Korea*

[3]*College of Pharmacy and Research Institute of Life and Pharmaceutical Sciences, Sunchon National University, Jeonnam 57922, Republic of Korea*

[4]*Department of Pharmacy, Mokpo National University, Jeonnam 58554, Republic of Korea*

[5]*Department of Biomedicine, Health & Life Convergence Sciences, BK21 Four, Mokpo National University, Jeonnam 58554, Republic of Korea*

[6]*Department of Oriental Medicine Resources, Sunchon National University, Jeonnam 57922, Republic of Korea*

[7]*Chunsu Mountain Medicinal Herb Research Association, Gyeonggi-do 13637, Republic of Korea*

ABSTRACT

Objective: To isolate and identify active constituents from *Gracilaria chorda* extract prepared under subcritical water conditions at 210 ℃ (GCSW210) and evaluate their anti-obesity and anti-diabetic effects in 3T3-L1 adipocytes and high-fat diet (HFD)-induced obese zebrafish larvae.

Methods: GCSW210 was fractionated through solvent partitioning, ion-exchange chromatography, and silica gel medium-pressure liquid chromatography, followed by preparative high performance liquid chromatography. At each step, bioactivities were assessed in 3T3-L1 adipocytes by Oil Red O staining and 2-NBDG uptake assays. The most active fractions were further purified, and isolated compounds were tested in HFD-induced obese zebrafish larvae.

Results: Liquid chromatography-hyphenated analysis with reference standards identified two major compounds in GCSW210: 5-hydroxymethylfurfural and bis(5-formylfurfuryl) ether. Both compounds significantly inhibited lipid accumulation in 3T3-L1 adipocytes and modulated gene expression associated with adipogenesis, glucose metabolism, and inflammation in zebrafish. They also enhanced glucose uptake, reduced circulating glucose levels, and improved insulin sensitivity. Notably, the effects were comparable to those of the crude GCSW210 extract. *In silico* docking studies confirmed stable interactions of both compounds with key metabolic and inflammatory targets, with bis(5-formylfurfuryl) ether showing stronger binding affinities.

Conclusions: These findings suggest that 5-hydroxymethylfurfural and bis(5-formylfurfuryl) ether are key contributors to the therapeutic activity of *Gracilaria chorda*, highlighting its potential as a functional food ingredient for the prevention or management of metabolic disorders.

Summary

Question: What are the active ingredients in *Gracilaria chorda* subcritical water extract (GCSW210), and do they show anti-obesity and anti-diabetic effects?

Findings: 5-Hydroxymethylfurfural and bis(5-formylfurfuryl) ether isolated from the GCSW210 significantly reduced lipid accumulation, enhanced glucose uptake, and lowered blood glucose levels compared to the control group in 3T3-L1 adipocytes and high-fat diet-induced obese zebrafish larvae. Their effects were comparable to the crude extract GCSW210.

Meaning: 5-Hydroxymethylfurfural and bis(5-formylfurfuryl) ether are major bioactive compounds in GCSW210 with anti-obesity and anti-diabetic effects, supporting its potential as functional food ingredients for the management of metabolic disorders.

✉To whom correspondence may be addressed. E-mail: rhyudy69@gmail.com, rhyudy@mokpo.ac.kr (DY. Rhyu); minalee@scnu.ac.kr (M. Lee)

How to cite this article: Thakuri LS, Le D, Kim HJ, Kim JJ, Seo JB, Park JC, et al. *Gracilaria chorda*-derived compounds improve lipid metabolism and insulin sensitivity in 3T3-L1 adipocytes and high-fat diet-induced obese zebrafish larvae. Asian Pac J Trop Biomed 2025; 15(10): 407-419.

Article history: Received 21 July 2025; Revision 19 August 2025; Accepted 21 October 2025; Available online 29 October 2025

KEYWORDS: 5-Hydroxymethylfurfural; Bis(5-formylfurfuryl) ether; *Gracilaria chorda*; Obesity; Zebrafish larvae; Anti-diabetes

1. Introduction

Obesity is a multifaceted metabolic disorder characterized by the excessive accumulation of triglycerides (TG) in adipose tissue, primarily due to an increase in both the size and number of adipocytes[1]. As a growing global health concern, obesity affects people of all ages and socioeconomic backgrounds[2]. Rather than being linked to inherited lipid metabolism disorders, it typically arises from a chronic imbalance between calorie intake and expenditure, often worsened by sedentary lifestyles and poor dietary habits[3,4]. This metabolic disruption leads to the release of non-esterified fatty acids, glycerol, hormones, and pro-inflammatory cytokines from adipose tissue, all of which contribute to the onset of insulin resistance (IR)[5].

IR occurs when cells fail to respond effectively to insulin, a condition closely tied to obesity[6]. Elevated levels of free fatty acids and inflammatory cytokines such as tumor necrosis factor-α (TNF-α) and interleukin-6 (IL-6) interfere with insulin signaling pathways, thereby reducing glucose uptake and disturbing normal glucose homeostasis[7]. This results in hyperglycemia and compensatory hyperinsulinemia caused by impaired intracellular signaling[8]. Under normal physiological conditions, insulin initiates a cascade involving insulin receptor substrate-1 (IRS-1), phosphoinositide 3-kinase (PI3K), and protein kinase B (AKT), culminating in the translocation of glucose transporter type 4 (GLUT4) to the cell membrane for glucose uptake[9]. The PI3K/AKT pathway is, therefore, a critical target in managing IR and related metabolic conditions. Additionally, AMP-activated protein kinase (AMPK) serves as another key regulator by promoting insulin-independent glucose uptake. Activation of AMPK triggers GLUT4 expression and facilitates glucose transport into cells, offering an alternative pathway to improve insulin sensitivity[10,11]. Thus, targeting both PI3K/AKT and AMPK pathways represents a promising strategy for treating IR and obesity-related disorders.

Natural bioactive compounds are increasingly being explored for their ability to modulate these pathways. *Gracilaria chorda* (GC), a red seaweed traditionally consumed in Asia and Europe, is rich in vitamins, minerals, and bioactive peptides with reported anti-diabetic and anti-hypertensive effects[12]. Of particular interest are subcritical water extracts of GC prepared at 210 ℃ (GCSW210), which have shown potential to inhibit adipogenesis, reduce inflammation, and improve IR by enhancing glucose uptake in both cell-based and animal models[13–15]. However, the active constituents responsible for these effects remain largely unidentified. This study aimed to isolate and characterize the bioactive compounds in GCSW210 using chromatographic and spectroscopic techniques, and to evaluate their effects on adipogenesis and glucose metabolism in 3T3-L1 adipocytes and high-fat diet (HFD)-fed zebrafish larvae.

2. Materials and methods

2.1. Reagents

Dimethyl sulfoxide (DMSO), 3-(4,5-dimethylthiazol-2-yl)-2,5-diphenyl tetrazolium bromide (MTT), insulin, 3-isobutyl-1-methylxanthine (IBMX), dexamethasone (DEX), and Oil Red O were purchased from Sigma-Aldrich (St Louis, MO, USA). 2-[*N*-(7-nitrobenz-2-oxa-1,3-diazol-4-yl) amino]-2-deoxyglucose (2-NBDG) was purchased from Invitrogen (Carlsbad, CA, USA). All solvents and reagents were of analytical grade and purchased from Sigma-Aldrich, unless otherwise specified. High-performance liquid chromatography (HPLC)-grade solvents were purchased from Fisher Scientific (Hampton, NH, USA).

2.2. Preparation of GCSW210

GCSW210 was prepared as previously described[13]. Briefly, GC samples were collected, washed to remove excess salt, dried at 40 ℃, and then chopped into smaller pieces. Subcritical water extraction was performed using a botanical extraction equipment (TPR-1; TAIATSU TECHNO, Osaka, Japan). Chopped GC and tertiary distilled water were mixed and placed in the reaction cell of a subcritical water reactor. The reaction temperature was adjusted to 210 ℃, and maintained under a reaction pressure of 3 MPa for approximately 1 min. After the reaction, the extracts were cooled to room temperature, filtered under reduced pressure (110-mm filter paper, Whatman No.2), and freeze-dried. The final powdered extracts were stored at −20 ℃ until further use.

2.3. GCSW210 fractions

GCSW210 (98 g) was suspended in water (1 L) and partitioned with *n*-hexane (*n*-HEX) (1 L × 2), ethyl acetate (EtOAc) (1 L × 4), and *n*-butanol (*n*-BuOH) (1 L × 3) (Supplementary Figure 1). The EtOAc fraction (19 g) was further fractionated using ion-exchange chromatography. A resin bed (1 000 g) was soaked in MeOH (approximately 1.5 L), gently stirred, and left to rest for 15 min. After decanting MeOH and adding distilled water (final volume 5 L), five EtOAc fractions (A-E) were obtained. The EtOAc fractions (B and C) were subjected to Si gel medium-pressure liquid chromatography (MPLC) (Biotage Isolera One; Biotage, Uppsala, Sweden) using a 1∶1 ratio of chloroform to ethyl acetate/MeOH (1∶3) solution at a flow rate of 50 mL/min for 60 min, resulting in sub-fractions (S1-S8). The isolated sub-fraction S2 (0.53 g) was purified by preparative HPLC (Waters 600 system, Waters, Milford, MA) using a SunFire Prep OBD column (5 μm, 19 mm × 150 mm;

Waters) and a gradient of MeOH and 0.1% HCOOH-containing water (20:80 to 100% MeOH, 40 min) at a flow rate of 10.0 mL/min, yielding Peak 1 (0.35 g) and Peak 2 (0.12 g).

2.4. Liquid chromatography–photodiode array (LC–PDA) and liquid chromatography–mass spectrometry (LC–MS) analysis

LC-PDA was performed using a Shiseido CAPCELL PAK C18 MGII column (4.6 mm × 250 mm, 5 μm; Shiseido, Japan) as previously described[14]. GCSW210 and standard solutions were injected and eluted over 40 min at 1.0 mL/min using methanol, 0.1% formic acid in water, and acetonitrile (5%-15%), with UV detection at 280 nm.

For LC-MS, an Agilent 1260 Infinity system with a Zorbax Eclipse Plus C18 column (2.1 mm × 50 mm, 1.8 μm) was used. The gradient elution involved 0.1% formic acid in water and acetonitrile (2%-100%) over 15 min, followed by a 10 min acetonitrile wash at 0.2 mL/min. MS detection employed positive-mode electrospray ionization across an *m/z* range of 100-1 000.

2.5. Bioactivity of the isolated compounds

GCSW210 was separated into four solvent-based fractions, with the EtOAc fraction showing the most potent activity. This fraction was further divided into five sub-fractions (GCEtOAc-A to -E) *via* ion-exchange chromatography, followed by MPLC and preparative HPLC purification of active compounds from GCEtOAc-B and -C. Major HPLC peaks were isolated, identified, and tested for bioactivity in both models.

2.6. Cell culture and cell viability assay

3T3-L1 preadipocytes (ATCC, Manassas, VA, USA) were cultured in DMEM supplemented with 10% newborn calf serum and 1% penicillin-streptomycin. For adipogenic differentiation, cells were treated for 2 d with an induction medium containing 5 μg/mL insulin, 0.5 mM 3-isobutyl-1-methylxanthine, and 1 μM dexamethasone in DMEM with 10% fetal bovine serum, followed by a differentiation medium (5 μg/mL insulin in DMEM with 10% fetal bovine serum) changed every 2 days for 8 d[16].

Cell viability was assessed using the MTT assay. Cells were seeded in 96-well plates (1×10^4 cells/well) and treated with GCSW210 fractions (125-500 μg/mL), sub-fractions (62.5-250 μg/mL), or isolated compounds (25-200 μM) during the 8-day differentiation period. After treatment, 1 mg/mL MTT solution was added and incubated for 3 h. Formazan crystals were solubilized with DMSO, and absorbance was measured at 540 nm using a microplate reader (Immuno Mini NJ-2300).

2.7. Oil Red O staining

The fat-soluble dye Oil Red O was used to investigate the intracellular lipid accumulations. Differentiated adipocytes were washed twice with phosphate-buffered saline (PBS) and then fixed for 30 min at 25 ℃ with 10% formalin in PBS. Then, cells were washed twice with PBS and stained with a filtered Oil Red O solution (0.5% in 60% isopropanol) for 1 h. Finally, cells were washed twice with distilled water, and fat droplets in 3T3-L1 adipocytes were observed *via* phase-contrast microscopy. Next, 1 mL of 100% isopropanol was added to each well for 15 min, and TG was measured at 540 nm (Immuno Mini NJ- 2300).

2.8. Glucose uptake analysis

Glucose uptake was monitored by 2-NBDG assay. Differentiated 3T3-L1 adipocytes were treated with the fractions or isolated compounds of GCSW210 for 24 h, followed by treatment with 2-NBDG dissolved in PBS and incubation for 30 min. Fluorescence intensity was measured using a fluorescence microplate reader (Perkin Elmer, Waltham, MA, USA) at excitation and emission wavelengths of 485 and 535 nm, respectively.

2.9. Zebrafish husbandry and toxicity assay

Wild-type *Danio rerio* (AB line) purchased from Korea Zebrafish Reseaource Center (Jeonnam, South Korea) were maintained at 28 ℃ (14 h light/10 h dark cycle, pH 7.0) in a flow-through system (Zebtec, Techniplast, Italy). Fertilized embryos were collected 6 h post-fertilization and cultured in E2 medium. On day 6 post-fertilization (dpf), larvae were exposed to isolated compounds (0.5, 5, and 50 μM) for 24 h. Morphology and viability were evaluated using a LEICA MZ10F microscope by assessing structural features (yolk sac, jaw, eyes, tail), and malformation and mortality rates were recorded as previously described[17].

2.10. Feeding protocol for HFD–induced obese zebrafish larvae

For obese zebrafish, a previously described protocol[18] was followed with some modifications. Briefly, on 5 dpf, zebrafish larvae were pre-selected, transferred to a petri-dish, and divided into 4 groups, including a control group. A petri dish (150 mm × 25 mm) contained 50 mL of E2 medium with 40 larvae in each group. For the control group, Gemma Micro ZF 75 diet was fed, and for the HFD group, 1 mg/mL chicken egg yolk (Sigma-Aldrich) diluted in E2 medium (final concentration 0.4%) was administered. Larvae were treated with GCSW210 extracts (250 μg/mL) or 50 μM isolated compounds [5-hydroxymethylfurfural (5-HMF) and bis(5-

formylfurfuryl) ether (bis-5FE)] along with an HFD solution till 9 dpf. All feeds were prepared and changed according to the required final volume and concentration. Larvae were fasted overnight before being collected for further experiments.

2.11. Measurement of body weight and glucose levels

A pool of 10 larvae was used to measure body weight, which was calculated by removing the weight of water from the weight of the pool. For measuring glucose level, 30-40 larvae from each group were homogenized using a Bullet Blender™ (Next Advance Lab Products, Palmer, MA, USA) within a Capped-Eppendorf tube using zirconium oxide beads (0.5 mm). After homogenization, the supernatant was collected in a fresh tube, and glucose level was measured using a glucose assay kit, according to the manufacturer's instructions (Asanpharm, South Korea). Glucose level was calculated using the following formula:

Glucose level = (Absorbance of sample/ Absorbance of standard) × 200 mg/dL

2.12. Glucose uptake by zebrafish

To measure glucose uptake, zebrafish larvae were exposed to 100 μL 2-NBDG (600 μM) and incubated for 3 h in the dark. Then, zebrafish larvae were washed three times with E2 medium. Larvae from each group were anaesthetized with MS-222 (Tricaine, CAS: 888-86-2; Sigma-Aldrich). Images of larvae were captured at 40× magnification using a LEICA MZ10F microscope (Leica) equipped with a mounted camera and iSolution software. Fluorescence intensity of each zebrafish larva was quantified using ImageJ (National Institutes of Health, Bethesda, MD, USA).

2.13. Whole-mount Oil Red O staining

After overnight fasting, zebrafish larvae were fixed overnight with 4% paraformaldehyde at 4 ℃ and washed thrice. Subsequently, zebrafish larvae were consecutively immersed in 85% and 100% 1,2-propanediol at room temperature for 20 min. Then, a fresh 0.5% Oil Red O solution was added, and zebrafish larvae were dyed at room temperature for 4 h. The larvae were consecutively washed with 100% and 85% 1,2-propanediol. Finally, lipid droplets in the liver tissue were observed and photographed. Images of the larvae were captured using a LEICA MZ10F microscope (Leica) equipped with a mounted camera and iSolution software.

2.14. Quantitative real-time polymerase chain reaction (qRT-PCR)

Zebrafish larvae were homogenized using a Bullet Blender homogenizer, and total RNA was extracted using TRIzol reagent (Molecular Research Center, OH, USA), according to the manufacturer's instructions. RNA was quantified using a NanoDrop spectrophotometer (Keen Innovative Solutions, South Korea). Primers were purchased from Integrated DNA Technologies (IA, USA). qRT-PCR analysis was performed using SYBR Green on an Applied Biosystems StepOne™ Real-Time PCR System Thermal Cycling Block (Applied Biosystems, USA). The base sequences of the oligonucleotide primers are listed in Supplementary Table 1. The thermal cycle was 95 ℃ for 15 min initial denaturation, followed by denaturation at 95 ℃ for 20 s, and elongation and conjugation for 30 s at 57 ℃, for 40 cycles. Glyceraldehyde 3-phosphate dehydrogenase (*GAPDH*) was used as an internal control to normalize the relative expression of genes. Relative gene expression was quantified using the $2^{-\Delta\Delta CT}$ method.

2.15. Molecular docking

The crystal structures of target proteins such as PPARγ (PDB ID: 4EMA), C/EBPα (PDB ID: 1NWQ), TNF-α (PDB ID: 2AZ5), IL-6 (PDB ID: 1ALU), and FOXO1 (PDB ID: 3CO6) were retrieved from the RCSB protein data bank (https://www.rcsb.org; accessed on February 3, 2025). The MGL tools 1.5.6 were updated to include each protein. After that, it was treated by adding polar hydrogen atoms, Kollman charges, and purifying the water and heteroatoms. The protein was saved in pdbqt format following the last stage of the receptor's preparation. Reference compounds and the structures of 5-HMF and bis-5FE were obtained in SDF formats from PubChem (https://pubchem.ncbi.nlm.nih.gov, October 26, 2024). They were then converted into appropriate pdbqt forms using the Open Babel software. Each structure was then put through MGL tools 1.5.6, and Gasteiger charges were applied to prepare them. The Pymol software was used to set the grid box specifications. AutoDock 4.2.6's Lamarckian genetic method was used to find the ligands' optimal conformation. The resulting complexes were established and visualized by using Discovery Studio Visualizer 2021 and PyMOL programs.

2.16. Statistical analysis

Statistical analyses were performed using GraphPad Prism v.8.0.2 (GraphPad Software, Inc., San Diego, CA, USA), followed by one-way analysis of variance (ANOVA) with Dunnett's test. Data are expressed as mean ± standard error of the mean (SEM). Statistical significance was defined as $P < 0.05$.

2.17. Ethical statement

All studies were approved by the Animal Experiment Ethics Committee of Mokpo National University, South Korea (Approval

No. MNU-IACUC-2025-008, approved on 27, May 2025) and conducted in accordance with the laboratory animal care guidelines of Mokpo National University and the American Veterinary Medical Association.

3. Results

3.1. Comparison of the effects of different GCSW210 fractions

To investigate the anti-adipogenic potential of GCSW210 and its four distinct fractions, 3T3-L1 preadipocytes were differentiated into adipocytes in the presence or absence of each fraction (Figure 1). As shown in Figure 1A, no significant cytotoxic effects were observed for any of the fractions, even at a concentration of 250 μg/mL. Notably, treatment with 250 μg/mL *n*-HEX [(119.32 ± 1.63)%] and EtOAc [(123.03 ± 1.59)%] fractions significantly enhanced glucose uptake in 3T3-L1 adipocytes (Figure 1B). Among them, the *n*-HEX [(50.96 ± 0.62)%] and EtOAc [(60.20 ± 3.87)%] fractions at 250 μg/mL significantly inhibited lipid accumulation compared to the other fractions (Figure 1C and D). Based on the observed inhibition of lipid accumulation and the promotion of glucose uptake, the anti-diabetic effects of the *n*-HEX and EtOAc fractions were comparable to those of crude GCSW210. However, due to the limited availability of the *n*-HEX fraction, further isolation and characterization were carried out using the EtOAc fraction.

3.2. Fractionation and the effects of GCSW210 EtOAc fraction

Ion-exchange chromatography using 19 g of the EtOAc fraction yielded five sub-fractions: GCEtOAc-A (1.61 g), GCEtOAc-B (4.20 g), GCEtOAc-C (1.70 g), GCEtOAc-D (2.28 g), and GCEtOAc-E (1.27 g). However, due to its high toxicity, GCEtOAc-E was excluded from further experiments. Subsequent assays were performed using the remaining sub-fractions to identify individual bioactive compounds (Figure 2). Among them, the GCEtOAc-C sub-fraction exhibited the most prominent effects, significantly inhibiting lipid accumulation and enhancing glucose uptake, without showing notable cytotoxicity. Treatment with GCEtOAc-B also resulted in a substantial increase in glucose uptake, along with a marked reduction in lipid accumulation and TG (Figure 2).

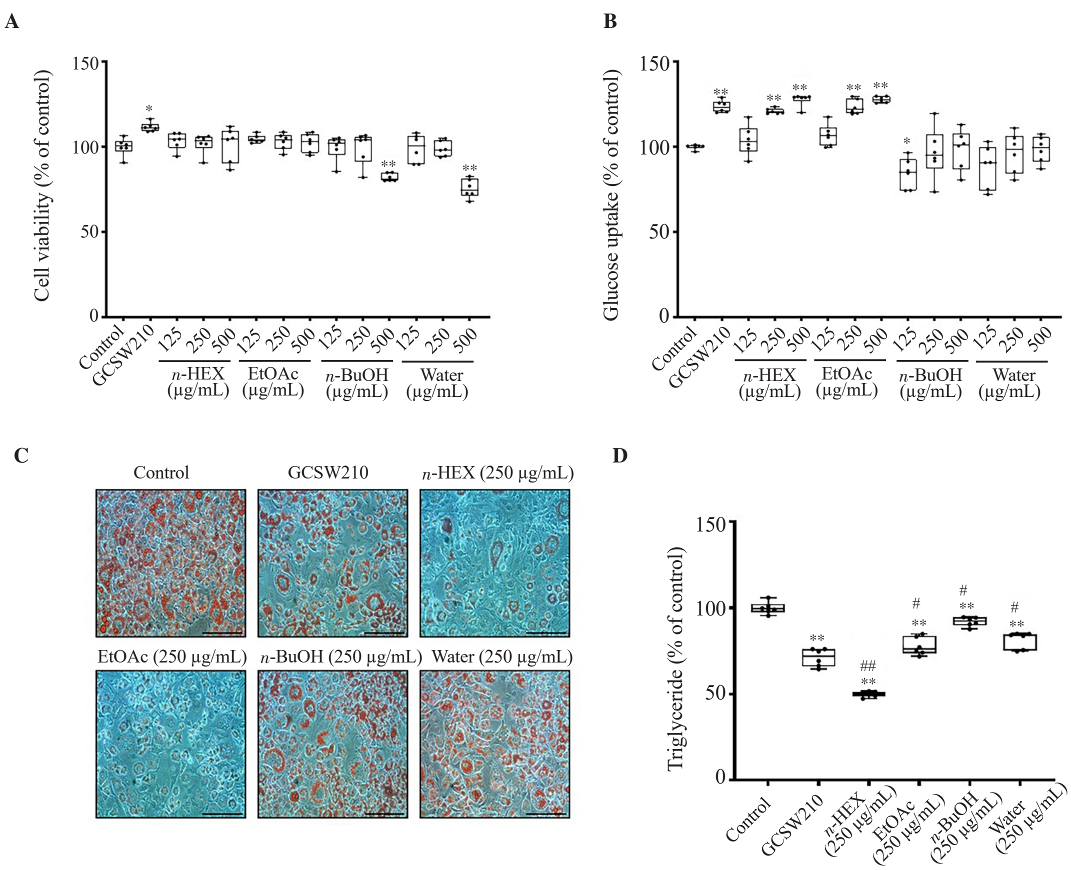

Figure 1. Effects of GCSW210 fractions on 3T3-L1 adipocytes. (A) Cell viability; (B) glucose uptake after treatment with four fractions of GCSW210; (C) Oil Red O stain (magnification: 200×; scale bar = 100 μm); (D) triglyceride content. The concentration of GCSW210 was 250 μg/mL. Data are presented as mean ± standard error of mean (SEM) (n = 6) and analyzed by one-way ANOVA followed by Dunnett's test. $^{*}P < 0.05$, $^{**}P < 0.001$ *vs.* control; $^{\#}P < 0.05$, $^{\#\#}P < 0.001$ *vs.* GCSW210. GCSW210: *Gracilaria chorda* under subcritical water conditions at 210 ℃.

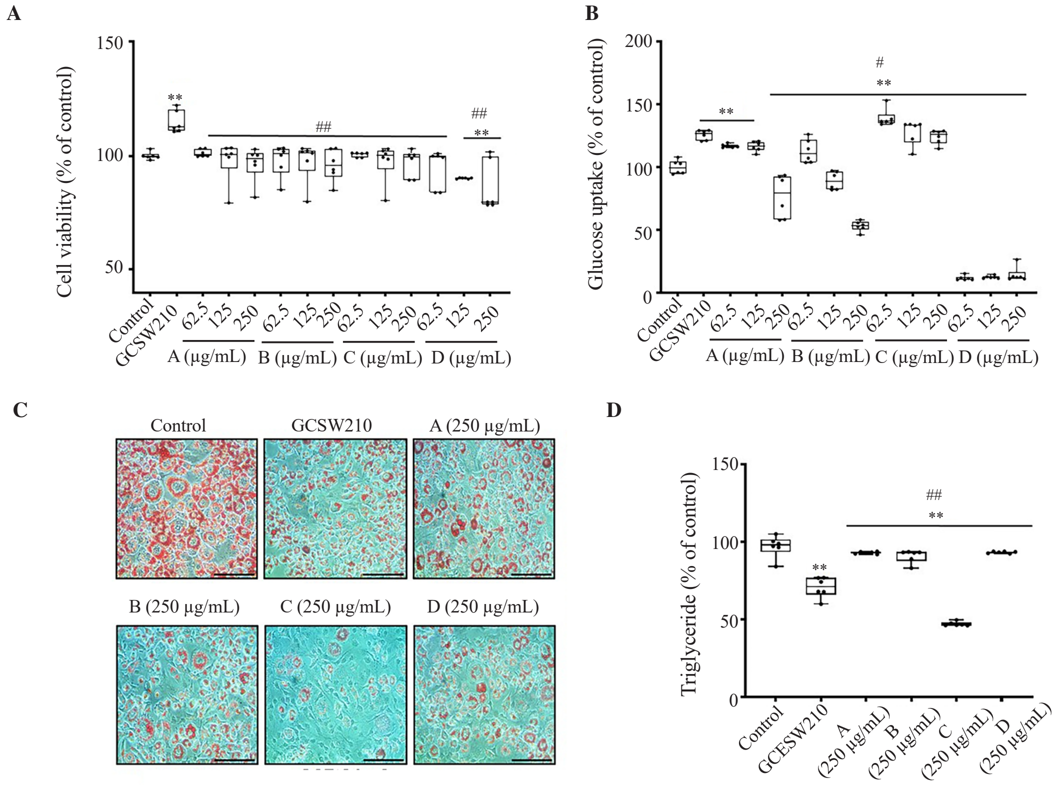

Figure 2. Effects of EtOAc fractions of GCSW210 (GCEtOAc) on 3T3-L1 adipocytes. (A) Effect of different GCEtOAc fractions on cell viability; (B) glucose uptake; (C) Oil Red O staining (magnification: 200×; scale bar = 100 μm); (D) triglyceride content. The concentration of GCSW210 was 250 μg/mL. Data are presented as mean ± SEM (n = 6) and analyzed by one-way ANOVA followed by Dunnett's test. $^{**}P < 0.001$ *vs.* control; $^{\#}P < 0.05$, $^{\#\#}P < 0.001$ *vs.* GCSW210.

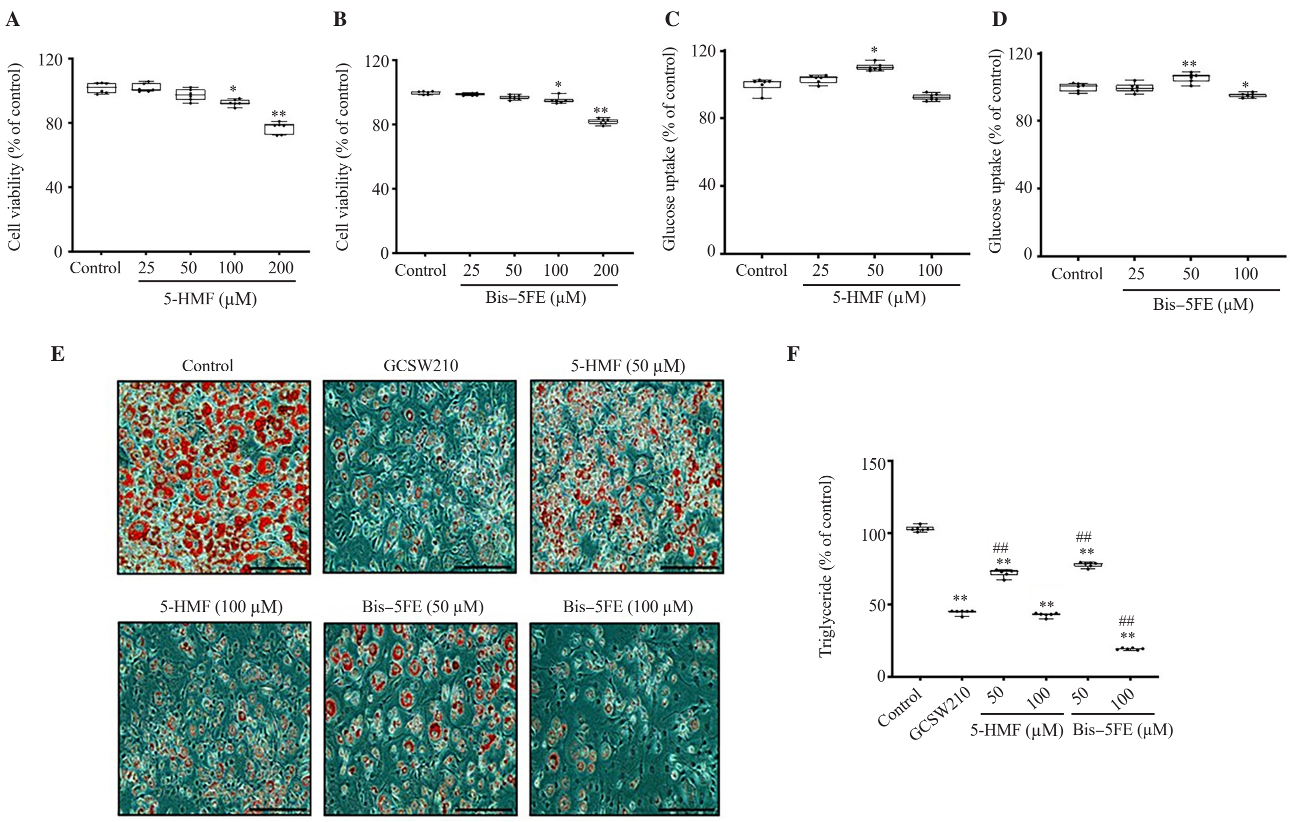

Figure 3. Effects of the isolated compounds of GCSW210 on 3T3-L1 adipocytes. (A-B) Cytotoxicity of 5-hydroxymethylfurfural (5-HMF) and bis(5-formylfurfuryl) ether (bis-5FE); (C-D) glucose uptake after treatment with 5-HMF or bis-5FE; (E) Oil Red O staining (magnification: 200×; scale bar = 100 μm); (F) triglyceride content. The concentration of GCSW210 was 250 μg/mL. Data are presented as mean ± SEM (n = 6) and analyzed by one-way ANOVA followed by Dunnett's test. $^{*}P < 0.05$, $^{**}P < 0.001$ *vs.* control; $^{\#\#}P < 0.001$ *vs.* GCSW210.

3.3. Isolation, purification, identification, and quantification of major compounds

Given the promising results of the GCEtOAc sub-fractions, further isolation was conducted. MPLC was employed to analyze the GCEtOAc-B and GCEtOAc-C fractions, which were subsequently purified using preparative HPLC to isolate two peaks: Peak 1 (Rt 3.49) and Peak 2 (Rt 12.91). In the HPLC chromatogram of GCSW210, these compounds appeared as major peaks. As shown in Supplementary Figure 2, Peak 1 exhibited UV absorption (UV_{max} 284.2 nm) and mass spectrometry (*m/z* 127.1 $[M+H]^+$) characteristics consistent with 5-HMF. Furthermore, the main LC peak of GCSW210 appeared at a very similar retention time (Rt 3.49) to that of 5-HMF (Rt 3.39) under identical conditions. The content of 5-HMF in GCSW210 was quantified as (49.42 ± 1.97) mg/g using a calibration curve constructed with a 5-HMF standard. Similarly, another LC peak of GCSW210 appeared at a retention time of 12.91, closely matching that of bis-5FE (Rt 12.90) under the same conditions, with a UV absorption maximum at 283.0 nm. The content of bis-5FE in GCSW210 was determined to be (9.03 ± 4.71) mg/g based on a calibration curve using a bis-5FE standard. Structural identification of bis-5FE was performed using NMR

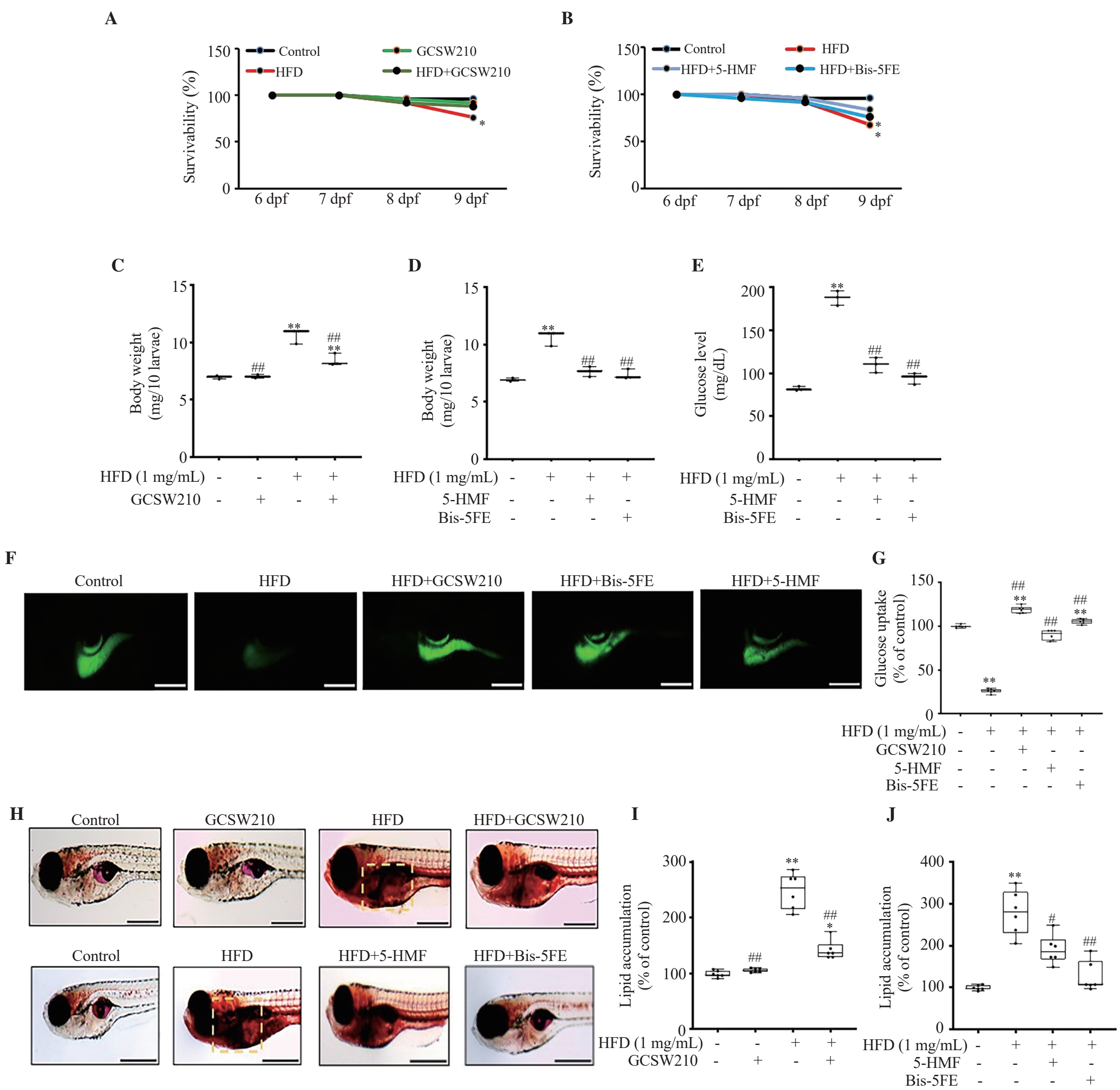

Figure 4. Effects of GCSW210 and its compounds in high fat diet (HFD)-induced obese zebrafish: (A-B) Survival rate; (C-D) body weight; (E) glucose levels; (F) glucose uptake imaging (magnification: 50×, scale bar = 100 μm); (G) glucose uptake quantification; (H-J) lipid accumulation (Oil Red O; magnification: 50×; scale bar = 50 μm). Groups: Control, HFD control (1 mg/mL egg yolk), HFD+GCSW210 (250 μg/mL), HFD plus 5-HMF/bis-5FE (50 μM). Yellow dotted boxes indicate stained liver sections. Data are expressed as mean ± SEM (*n*=3-6) and analyzed by one-way ANOVA followed by Dunnett's test. $^{*}P < 0.05$, $^{**}P < 0.001$ *vs*. control; $^{\#}P < 0.05$, $^{\#\#}P < 0.001$ *vs*. HFD-fed group. dpf: days post-fertilization.

spectroscopy (Supplementary Figure 3).

3.4. Effects of isolated compounds in 3T3–L1 adipocytes

Both 5-HMF and bis-5FE showed slight cytotoxicity at 100 μM concentration on 3T3-L1 adipocytes [5-HMF: (91.30 ± 0.76)%; bis-5FE: (90.12 ± 0.84)%] (Figure 3A and B). At 50 μM, both compound induced significant intracellular glucose uptake (Figure 3C and D). Additionally, 5-HMF and bis-5FE exhibited remarkable efficacy in inhibiting lipid accumulation during adipocyte differentiation (Figure 3E and F). Nevertheless, the effects of 5-HMF and bis-5FE were comparable to those previously observed for the crude extract[13].

3.5. Effects of isolated compounds on HFD–induced obese zebrafish larvae

Zebrafish larvae exposed to 1 mg/mL HFD showed a decreased survival rate to approximately 76%. Notably, larvae treated with GCSW210 (250 μg/mL), 5-HMF (50 μM), or bis-5FE (50 μM) along with HFD showed a higher survival rate than the group treated with HFD only (Figure 4A and B). As expected, the metabolic parameters, like body weight, were significantly elevated in HFD-induced obese larvae [(10.63 ± 0.37) mg/10 larvae] (Figure 4C and D). Notably, the body weight of the bis-5FE group [(7.12 ± 0.26) mg/10 larvae] was lower than that in the 5-HMF group [(7.67 ± 0.20) mg/10 larvae]. Moreover, the HFD-induced group showed an elevated intracellular glucose level [(195.63 ± 0.32) mg/dL], a hallmark of IR compared to that of the control group (Figure 4E). Notably, both 5-HMF and bis-5FE significantly reduced HFD-induced glucose levels to [(99.35 ± 0.81) mg/dL] and [(97.41 ± 0.82) mg/dL], respectively. Glucose uptake was drastically reduced in the HFD group [(25.08 ± 1.14)%], confirming impaired glucose metabolism and development of IR. HFD-induced obese larvae treated with GCSW210, 5-HMF, or bis-5FE demonstrated a significant increase in glucose uptake (Figure 4F and G). Furthermore, lipid accumulation around the abdomen of HFD-treated larval zebrafish increased significantly (Figure 4H).

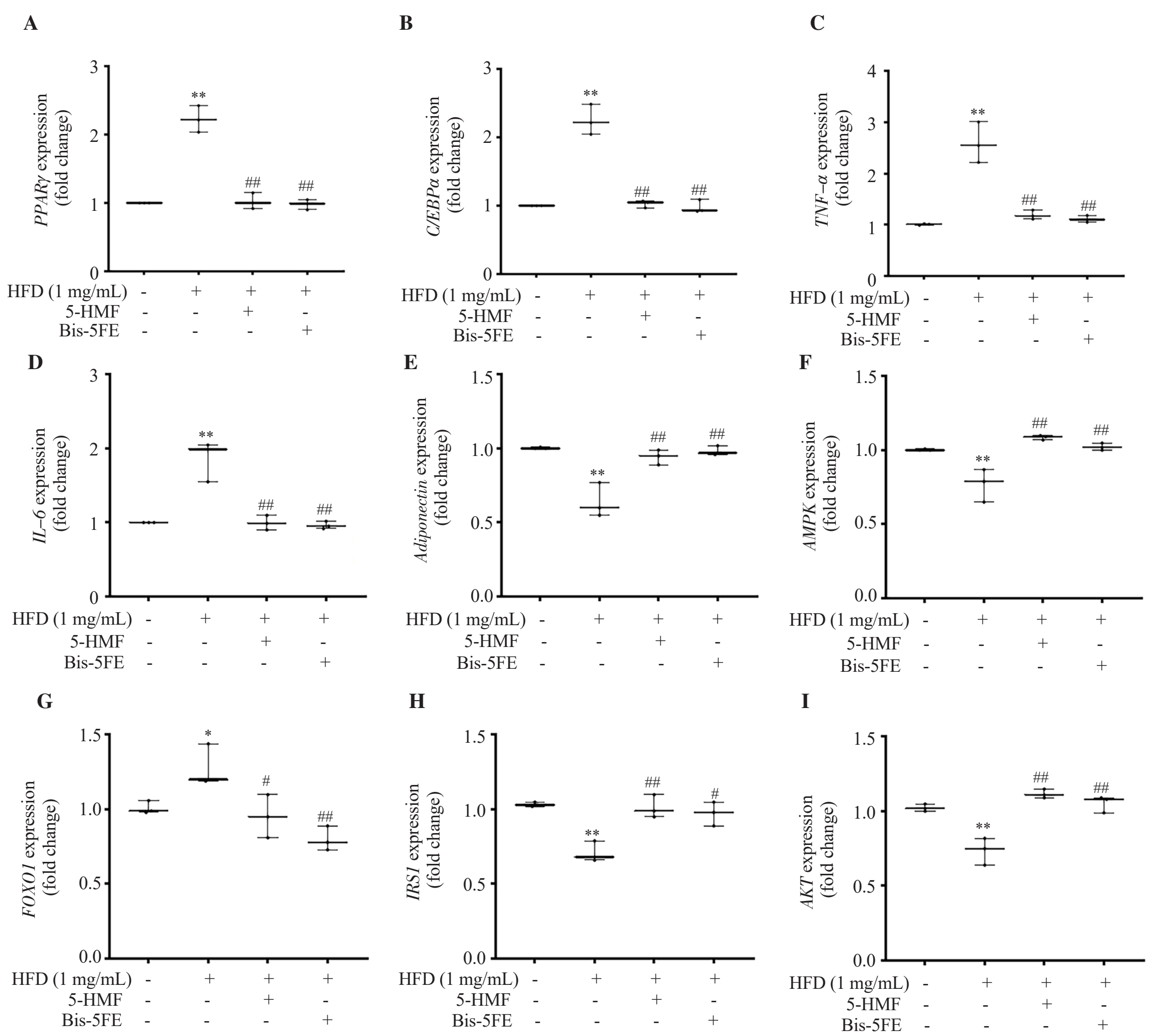

Figure 5. Effects of the isolated compounds on mRNA expression of genes related to fat and glucose metabolism in HFD-fed zebrafish larvae. Data are presented as mean ± SEM of three independent experiments and analyzed by one-way ANOVA followed by Dunnett's test. $^{*}P < 0.05$, $^{**}P < 0.001$ *vs.* control; $^{\#}P < 0.05$, $^{\#\#}P < 0.001$ *vs.* HFD-fed group.

Lipid staining around the liver section was dramatically reduced by treatment with 50 μM of the isolated compounds. Quantitative analysis showed that GCSW210 decreased lipid accumulation to approximately 55% of the HFD-fed group, while treatment with 5-HMF and bis-5FE markedly reduced lipid accumulation to approximately 64% and 53% of the HFD control, respectively (Figure 4I and J), suggesting that the anti-obesity effects of GCSW210 may be attributed to its compounds.

3.6. Effects of isolated compounds on mRNA expression of genes related to lipid and glucose metabolism

HFD-induced obesity in larvae led to increased expression of genes related to fat storage, specifically peroxisome proliferator-activated receptor gamma (*PPARγ*, 2.25 ± 0.12) and CCAAT/enhancer-binding protein α (*C/EBPα*, 2.23 ± 0.01) (Figure 5A and B). However, treatment with 5-HMF and bis-5FE significantly reduced the expression of these genes [*PPARγ*: (1.02 ± 0.06); *C/EBPα*: (1.03 ± 0.03)] and [*PPARγ*: (0.98 ± 0.05); *C/EBPα*: (0.98 ± 0.04)]. Furthermore, HFD caused an elevation in the levels of pro-inflammatory cytokines like *TNF–α* (2.59 ± 0.23) and *IL–6* (1.86 ± 0.15), which was also counteracted by the application of 5-HMF and bis-5FE (Figure 5C and D). An elevated expression of forkhead box O1 (*FOXO1*) was observed in the HFD group (1.28 ± 0.08) (Figure 5G). However, groups treated with the isolated compounds showed significantly decreased *FOXO1* expression compared with that of the HFD group, indicating their protective effects against IR induced by HFD. Similarly, the HFD group showed a notable downregulation

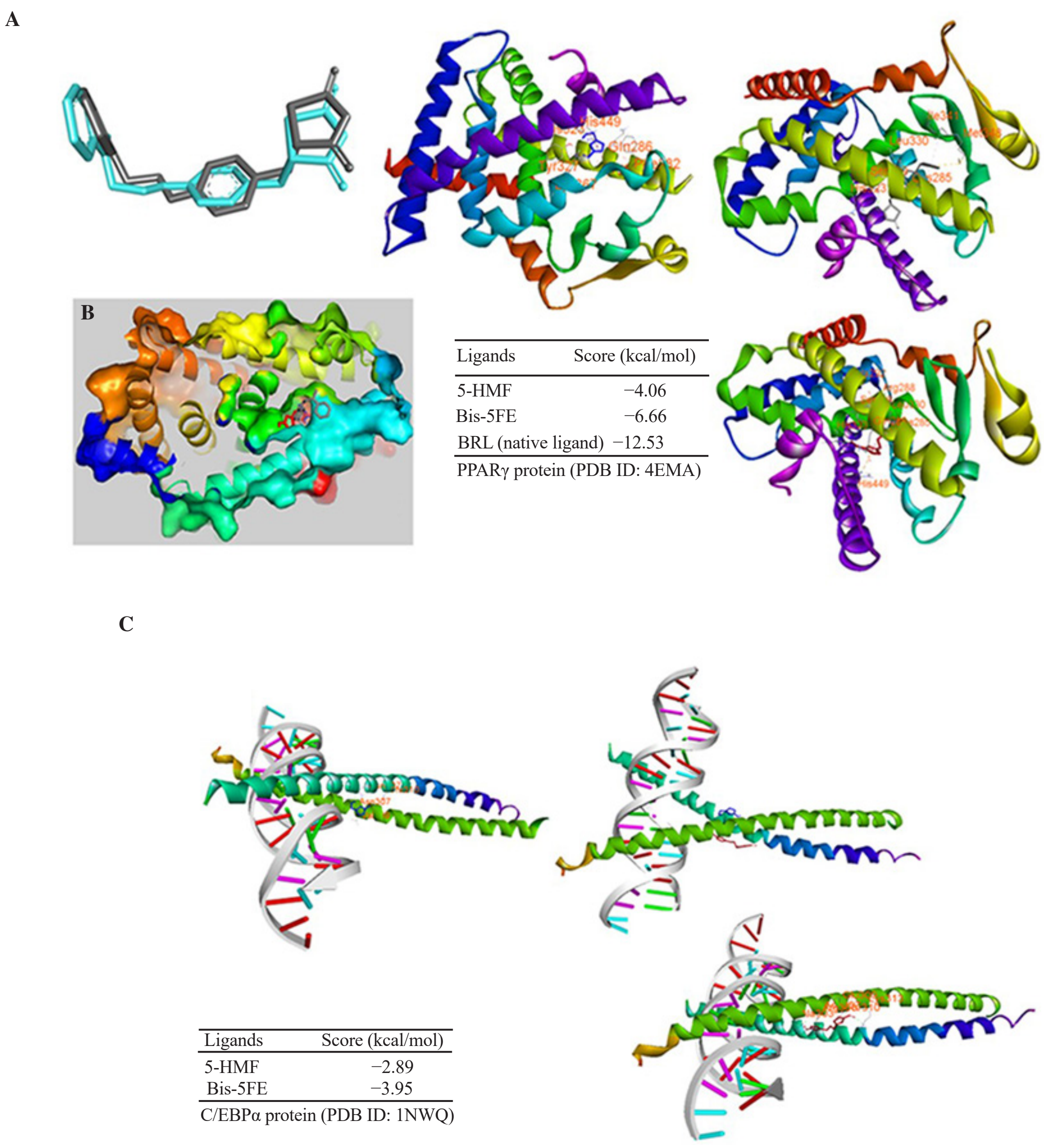

Figure 6. Superimposed native ligand (A) and compounds docked into binding pose (B). Ligand interactions of 5-HMF (blue), bis-5FE (red), and BRL (grey), with amino acid when they were docked into PPARγ protein (PDB ID: 4EMA). (C) Interactions of 5-HMF (blue) and bis-5FE (red), when they were docked into C/EBPα protein (PDB ID: 1NWQ).

of *AMPK* (0.77 ± 0.06) compared with the control group; however, the expression was significantly increased by 5-HMF (1.09 ± 0.01) and bis-5FE (1.02 ± 0.01) treatment (Figure 5F). Additionally, a significant decrease in circulating *adiponectin* expression was observed in HFD-fed obese zebrafish larvae (0.64 ± 0.07) (Figure 5E). In contrast, the obese groups receiving 5-HMF and bis-5FE showed increased *adiponectin* mRNA expression [(0.94 ± 0.14) and (0.98 ± 0.09), respectively], compared with that of larvae fed an HFD. In addition, 5-HMF and bis-5FE also markedly upregulated the mRNA expression of genes related to glucose metabolism (*IRS1* and *AKT*) (Figure 5H and I). This firmly establishes that GCSW210 effectively enhances the regulation of fat and glucose metabolism.

3.7. In-silico prediction of 5-HMF and bis-5FE binding to target proteins

To validate the docking protocol, the native ligand BRL (2,4-thiazolidinedione derivative) was redocked into PPARγ (PDB ID: 4EMA)[19], yielding an RMSD of 0.92 Å, confirming protocol reliability (Figure 6A). Both 5-HMF and bis-5FE occupied the same binding pocket as the native ligand (Figure 6B). Bis-5FE showed stronger binding affinity (ΔG = −6.66 kcal/mol) than 5-HMF (ΔG = −4.06 kcal/mol), forming hydrogen bonds with SER289 and HIS323, while 5-HMF interacted with HIS323 and TYR327. Both compounds also showed π-cation interactions with HIS449, amide π-stacking with CYS285, and van der Waals interactions with GLN286, PHE363, LYS367, LEU469, and TYR473.

Docking to C/EBPα (PDB ID: 1NWQ)[20] revealed that bis-5FE (ΔG = −3.95 kcal/mol) formed hydrogen bonds with ASN307, THR310, and LYS313, and hydrophobic contacts with ALA303, ARG306, and GLU309. In contrast, 5-HMF (ΔG = −2.89 kcal/mol) formed hydrogen bonds with ASN307 and THR310 and interacted hydrophobically with VAL308, THR310, and GLN311 (Figure 6C).

When docked into TNF-α[21], both compounds occupied the same

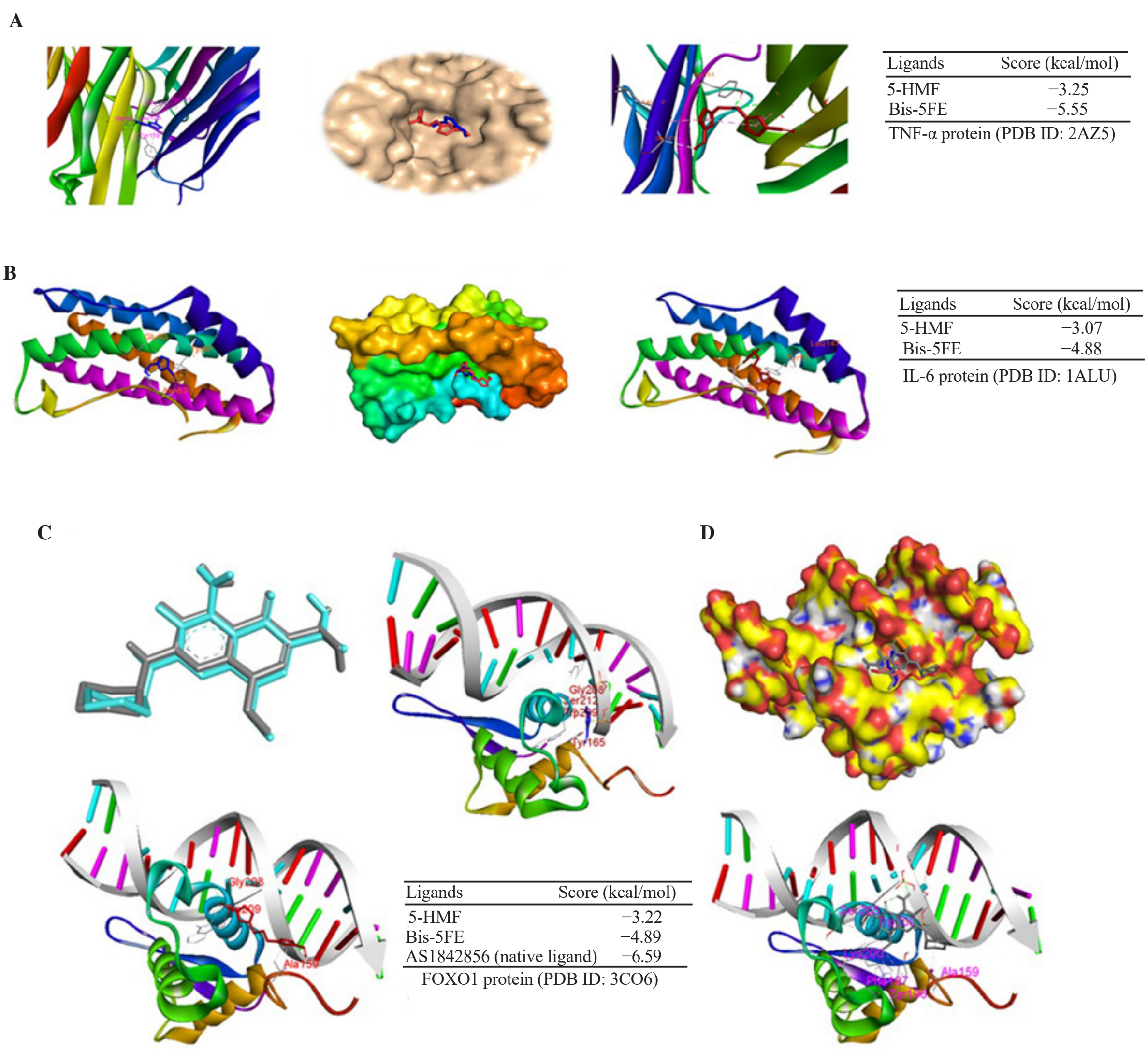

Ligands	Score (kcal/mol)
5-HMF	−3.25
Bis-5FE	−5.55
TNF-α protein (PDB ID: 2AZ5)	

Ligands	Score (kcal/mol)
5-HMF	−3.07
Bis-5FE	−4.88
IL-6 protein (PDB ID: 1ALU)	

Ligands	Score (kcal/mol)
5-HMF	−3.22
Bis-5FE	−4.89
AS1842856 (native ligand)	−6.59
FOXO1 protein (PDB ID: 3CO6)	

Figure 7. Docking interactions of 5-HMF (blue) and bis-5FE (red): (A) Binding poses in TNF-α (PDB: 2AZ5); (B) IL-6 (PDB: 1ALU); (C) superimposed with AS1842856 (grey) in FOXO1 (PDB: 3CO6) with binding scores; (D) electrostatic surface of FOXO1 showing ligand conformations.

site, with bis-5FE again showing stronger affinity (ΔG = −5.55 kcal/mol) than 5-HMF (ΔG = −3.25 kcal/mol). Bis-5FE formed hydrogen bonds with SER60, GLY121, and TYR151, and 5-HMF interacted with SER60, LEU120, GLY121, and TYR151, along with van der Waals contacts at TYR59, GLN61, and TYR119 (Figure 7A).

In IL-6 (PDB ID not specified[21]), bis-5FE also exhibited higher affinity (ΔG = −4.88 kcal/mol) than 5-HMF (ΔG = −3.07 kcal/mol). Both compounds bound ASN63 and TYR97 *via* hydrogen bonds, and interacted with LEU62, LEU64, PRO65, and GLU93 through hydrophobic forces. Bis-5FE also engaged in π-alkyl (LEU147), π-sigma (ASN63), and van der Waals interactions (Figure 7B).

Docking to FOXO1 (PDB ID: 3CO6)[22] was validated by redocking the native inhibitor AS1842856 (RMSD = 1.323 Å; Figure 7C). Bis-5FE showed stronger affinity (ΔG = −4.89 kcal/mol) than 5-HMF (ΔG = –3.22 kcal/mol), forming hydrogen bonds with GLY208 and TRP209, and hydrophobic interactions with ARG157, ASN158, ALA159, TRP160, TYR165, TYR196, SER205, and SER206[22]. 5-HMF formed hydrogen bonds with TYR165 and SER212, and additional van der Waals and π-stacking interactions with TRP160, TYR196, PHE197, LYS200, and GLY208 (Figure 7D).

Together, these findings demonstrate that bis-5FE consistently exhibits stronger binding affinities and broader interaction profiles across all target proteins compared to 5-HMF, supporting its greater therapeutic potential in regulating adipogenesis, inflammation, and IR.

4. Discussion

In this study, 5-HMF and bis-5FE were identified as the major bioactive constituents of GCSW210. These compounds exhibited comparable anti-diabetic and anti-obesity effects to the crude extract in both *in vitro* and *in vivo* models.

Previous studies have shown that GCSW210 inhibits lipid accumulation and regulates lipid and glucose metabolism *in vitro* and *in vivo*, supporting its anti-obesity and anti-diabetic potential. However, the active compounds responsible for these effects had not been identified. In this study, 5-HMF, a sugar degradation product, was identified as a major constituent and has been reported to prevent cardiovascular disease, diabetes, and inflammation[23] as well as exert hepatoprotective effects[24]. Another key compound, bis-5FE, a derivative of 5-HMF, has been described as a pre-polymer and antiviral precursor[25], with anti-inflammatory and anti-rheumatic activities[26,27]. These findings suggest that both 5-HMF and bis-5FE may contribute to the therapeutic potential of GCSW210 in metabolic disorders.

In 3T3-L1 adipocytes, both 5-HMF and bis-5FE significantly suppressed lipid accumulation and restored glucose uptake. Similarly, in HFD-induced obese zebrafish larvae, treatment with these compounds reduced glucose levels, inhibited adipogenic gene expression (*PPARγ* and *C/EBPα*), and downregulated pro-inflammatory cytokines (*TNF-α* and *IL–6*), indicating their ability to improve IR and metabolic dysregulation. Mechanistically, both compounds restored the expression of *IRS1* and *AKT*, key components of the insulin signaling pathway, and activated AMPK, a crucial energy-sensing kinase that enhances insulin-independent glucose uptake and inhibits lipogenesis[28]. Upregulation of adiponectin, a hormone known to improve insulin sensitivity and suppress SREBP-mediated lipogenesis *via* AMPK activation[29,30], further supported the insulin-sensitizing and anti-inflammatory actions of the compounds. Additionally, the compounds reduced the expression of *FOXO1*, a transcription factor associated with hepatic gluconeogenesis[31] and IR. Since FOXO1 plays a pivotal role in regulating gluconeogenesis, and its overactivation contributes to metabolic dysfunction and IR[32–34], its suppression highlights the potential of 5-HMF and bis-5FE to restore metabolic homeostasis under obesogenic conditions.

To complement these experimental findings, we performed *in silico* molecular docking to explore the binding interactions between the isolated compounds and key metabolic and inflammatory proteins[35]. Docking simulations revealed that bis-5FE exhibited stronger binding affinities than 5-HMF toward PPARγ, C/EBPα, TNF-α, IL-6, and FOXO1, through stable hydrogen bonding and hydrophobic interactions at key active site residues. These results align with the experimental findings and provide supportive evidence that both compounds may contribute to the biological activity of GCSW210.

In summary, this study suggests that 5-HMF and bis-5FE are potential bioactive agents capable of improving obesity- and IR-related metabolic dysfunction by modulating glucose and lipid metabolism, reducing inflammation, and restoring insulin signaling. These effects appear to involve both insulin-dependent (IRS1/AKT) and insulin-independent (AMPK) pathways, with molecular docking offering additional mechanistic support. Nevertheless, several limitations should be acknowledged. To utilize the two components isolated from GCSW210 as biomaterials, further studies on their physiological activity and acute and chronic toxicity under long-term exposure conditions in rodents are necessary. Additionally, metabolite profiling using UHPLC-MS/MS is essential to identify the various compounds present in GCSW210. Future studies should therefore assess safety, bioavailability, and efficacy in mammalian models, and formulation strategies such as nano-delivery systems may help enhance stability and therapeutic potential for managing metabolic disorders, including IR, obesity, and type 2 diabetes mellitus.

Conflict of interest statement

We declare that we have no conflict of interest.

Funding

This research was supported by the Basic Science Research Program of the National Research Foundation of Korea, funded by the Ministry of Education (2018R1D1A1B07050273). This work was supported by the National Research Foundation of Korea grant funded by the Korea government (Grant no.: RS-2022-NR070862). This research was supported (in part) by Glocal University Project of Mokpo National University in 2025.

Data availability statement

The data supporting the findings of this study are available from the corresponding authors upon request.

Authors' contributions

LST conducted the main investigation, including experimental design and analysis, and wrote original draft of manuscript. DDL was responsible for investigation and analysis. HJK also contributed to classification, identification, and data interpretation. JJK supervised aspects of the project and edited the manuscript. JBS contributed to editing. JCP and ML provided overall supervision. DYR conceptualized and supervised the study and contributed to manuscript review and editing. All authors reviewed and approved the final manuscript.

References

[1] Hristov I, Mocanu V, Zugun-Eloae F, Labusca L, Cretu-Silivestru I, Oboroceanu T, et al. Association of intracellular lipid accumulation in subcutaneous adipocyte precursors and plasma adipokines in bariatric surgery candidates. *Lipids Health Dis* 2019; **18**: 8. doi: 10.1186/s12944-019-1081-1089.

[2] Lin X, Li H. Obesity: Epidemiology, pathophysiology, and therapeutics. *Front Endocrinol (Lausanne)* 2021; **12**. doi: 10.3389/fendo.2021.706978.

[3] Martyn JA, Kaneki M, Yasuhara S, Warner DS, Warner MA. Obesity-induced insulin resistance and hyperglycemia: Etiologic factors and molecular mechanisms. *Anesthesiology* 2008; **109**: 137-148.

[4] Hruby A, Hu FB. The epidemiology of obesity: A big picture. *Pharmacoeconomics* 2015; **33**: 673-689.

[5] Kahn SE, Hull RL, Utzschneider KM. Mechanisms linking obesity to insulin resistance and type 2 diabetes. *Nature* 2006; **444**: 840-846.

[6] Kivimäki M, Strandberg T, Pentti J, Nyberg ST, Frank P, Jokela M, et al. Body-mass index and risk of obesity-related complex multimorbidity: An observational multicohort study. *Lancet Diabetes Endocrinol* 2022; **10**: 253-263.

[7] Ormazabal V, Nair S, Elfeky O, Aguayo C, Salomon C, Zuñiga FA. Association between insulin resistance and the development of cardiovascular disease. *Cardiovasc Diabetol* 2018; **17**: 122. doi: 10.1186/s12933-018-0762-4.

[8] Brown AE, Walker M. Genetics of insulin resistance and the metabolic syndrome. *Curr Cardiol Rep* 2016; **18**: 75. doi: 10.1007/s11886-016-0755-4.

[9] Boucher J, Kleinridders A, Kahn CR. Insulin receptor signaling in normal and insulin-resistant states. *Cold Spring Harb Perspect Biol* 2014; **6**. doi: 10.1101/cshperspect.a009191.

[10]Kahn BB. Glucose transport: Pivotal step in insulin action. *Diabetes* 1996; **45**: 1644-1654.

[11]Vlavcheski F, MacPherson RE, Tsiani E. Rosemary extract activates AMPK, inhibits mTOR and attenuates the high glucose and high insulin-induced muscle cell insulin resistance. *Appl Physiol Nutr Metab* 2021; **46**(7): 819-827.

[12]Mune Mune MA, Miyabe Y, Shimizu T, Matsui W, Kumagai Y, Kishimura H. Characterisation of bioactive peptides from red alga *Gracilariopsis chorda*. *Mar Drugs* 2023; **21**(1): 49. doi: 10.3390/md21010049.

[13]Thakuri LS, Park CM, Park JW, Kim HA, Rhyu DY. Subcritical water extraction of *Gracilaria chorda* abbreviates lipid accumulation and obesity-induced inflammation. *Algae* 2023; **38**(1): 81-92.

[14]Thakuri LS, Park CM, Kim HA, Kim HJ, Park JW, Park JC, et al. *Gracilaria chorda* subcritical water ameliorates hepatic lipid accumulation and regulates glucose homeostasis in a hepatic steatosis cell model and obese C57BL/6J mice. *J Ethnopharmacol* 2024; **320**. doi: 10.1016/j.jep.2023.117395.

[15]Thakuri LS, Park CM, Park JW, Rhyu DY. *Gracilaria chorda* subcritical-water extracts as ameliorant of insulin resistance induced by high-glucose in zebrafish and dexamethasone in L6 myotubes. *J Tradit Complement Med* 2024; **14**(1): 82-90.

[16]Park CH, Rhyu DY, Sharma BR, Yokozawa T. Inhibition of preadipocyte differentiation and lipid accumulation by 7-*O*-galloyl-*D*-sedoheptulose treatment in 3T3-L1 adipocytes. *Biomed Prev Nutr* 2013; **3**(4): 319-324.

[17]Thakuri LS, Kim JE, Choi JY, Rhyu DY. Protective effect of *Capsosiphon fulvescens* on oxidative stress-stimulated neurodegenerative dysfunction of PC12 cells and zebrafish larva models. *Fish Aquat Sci* 2023; **26**(1): 24-34.

[18]Den Broeder MJ, Moester MJ, Kamstra JH, Cenijn PH, Davidoiu V, Kamminga LM, et al. Altered adipogenesis in zebrafish larvae following high fat diet and chemical exposure is visualised by stimulated Raman scattering microscopy. *Int J Mol Sci* 2017; **18**(4): 894. doi: 10.3390/

ijms18040894.

[19]Le DD, Kim E, Dang T, Lee J, Shin CH, Park JW, et al. Chemical investigation and regulation of adipogenic differentiation of cultivated *Moringa oleifera*. *Pharmaceuticals* 2024; **17**. doi: 10.3390/ph17101310.

[20]Deepa VS, Kumar PS, Vadivukkarasi B, Tilton FL. Molecular docking studies on selected phytocompounds from different *Andrographis* sp against PPAR-γ and C/EBP-α receptors for type 2 diabetes. *Asian J Pharm Clin Res* 2013; **6**(2): 196-199.

[21]Choi J, Le DD, Roh N, Lee J, Shrestha D, Dinh T, et al. Chemical composition and biological activities of *Lagopsis supina* extract: Antioxidant, adipogenic, and anti-inflammatory effects. *Pharmaceuticals* 2025; **18**. doi: 10.3390/ph18020150.

[22]Damayanti DS, Utomo DH, Kusuma C. Revealing the potency of *Annona muricata* leaves extract as FOXO1 inhibitor for diabetes mellitus treatment through computational study. *In Silico Pharmacol* 2017; **5**: 3. doi: 10.1007/s40203-017-0023-3.

[23]Zhang H, Jiang Z, Shen C, Zou H, Zhang Z, Wang K, et al. 5-Hydroxymethylfurfural alleviates inflammatory lung injury by inhibiting endoplasmic reticulum stress and NLRP3 inflammasome activation. *Front Cell Dev Biol* 2021; **9**. doi: 10.3389/fcell.2021.782427.

[24]Li W, Qu XN, Han Y, Zheng SW, Wang J, Wang YP. Ameliorative effects of 5-hydroxymethyl-2-furfural (5-HMF) from *Schisandra chinensis* on alcoholic liver oxidative injury in mice. *Int J Mol Sci* 2015; **16**(2): 2446-2457.

[25]Casanova O, Iborra S, Corma A. Chemicals from biomass: Etherification of 5-hydroxymethyl-2-furfural (HMF) into 5,5′(oxy-bis(methylene))bis-2-furfural (OBMF) with solid catalysts. *J Catal* 2010; **275**(2): 236-242.

[26]Wang M, Li K, Nie Y, Wei Y, Li X. Antirheumatoid arthritis activities and chemical compositions of phenolic compounds-rich fraction from *Urtica atrichocaulis*, an endemic plant to China. *Evid Based Complement Alternat Med* 2012; **2012**. doi: 10.1155/2012/818230.

[27]Farzaei MH, Farzaei F, Gooshe M, Abbasabadi Z, Rezaei N, Abdolghaffari AH. Potentially effective natural drugs in treatment for the most common rheumatic disorder: Osteoarthritis. *Rheumatol Int* 2015; **35**: 799-814.

[28]Long YC, Zierath JR. AMP-activated protein kinase signaling in metabolic regulation. *J Clin Invest* 2006; **116**(7): 1776-1783.

[29]Khoramipour K, Chamari K, Hekmatikar AA, Ziyaiyan A, Taherkhani S, Elguindy NM, et al. Adiponectin: Structure, physiological functions, role in diseases, and effects of nutrition. *Nutrients* 2021; **13**(4). doi: 10.3390/nu13041180.

[30]Awazawa M, Ueki K, Inabe K, Yamauchi T, Kaneko K, Okazaki Y, et al. Adiponectin suppresses hepatic SREBP1c expression in an AdipoR1/LKB1/AMPK dependent pathway. *Biochem Biophys Res Commun* 2009; **382**(1): 51-56.

[31]Li X, Wan T, Li Y. Role of FoxO1 in regulating autophagy in type 2 diabetes mellitus (Review). *Exp Ther Med* 2021; **22**(1): 707. doi: 10.3892/etm.2021.10139.

[32]Luo L, Liu M. Adiponectin: Friend or foe in obesity and inflammation. *Med Rev* 2022; **2**(4): 349-362.

[33]Chen S, Villalta SA, Agrawal DK. FOXO1 mediates vitamin D deficiency-induced insulin resistance in skeletal muscle. *J Bone Miner Res* 2016; **31**(3): 585-595.

[34]Su D, Coudriet GM, Kim DH, Lu Y, Perdomo G, Qu S, et al. FoxO1 links insulin resistance to proinflammatory cytokine IL-1β production in macrophages. *Diabetes* 2009; **58**(11): 2624-2633.

[35]Agu PC, Afiukwa CA, Orji OU, Ezeh EM, Ofoke IH, Ogbu CO, et al. Molecular docking as a tool for the discovery of molecular targets of nutraceuticals in diseases management. *Sci Rep* 2023; **13**. doi: 10.1038/s41598-023-40160-2.

Publisher's note

Edited by Liang Q, Tan BJ